Current Performance and On-Going Improvements of the 8.2 m Subaru Telescope

Masanori Iye¹, Hiroshi Karoji², Hiroyasu Ando¹, Norio Kaifu³, Keiichi Kodaira⁴, Kentaro Aoki², Wako Aoki¹, Yoshihiro Chikada³, Yoshiyuki Doi², Noboru Ebizuka⁵, Brian Elms², Gary Fujihara², Hisanori Furusawa², Tetsuharu Fuse², Wolfgang Gaessler⁶, Sumiko Harasawa², Yutaka Hayano¹, Masahiko Hayashi², Saeko Hayashi², Shinichi Ichikawa¹ Masatoshi Imanishi¹, Catherine Ishida², Yukiko Kamata⁷, Tomio Kanzawa², Nobunari Kashikawa¹, Koji Kawabata¹, Naoto Kobayashi⁸, Yutaka Komiyama², George Kosugi², Tomio Kurakami², Michael Letawsky², Yoshitaka Mikami¹, Akihiko Miyashita², Satoshi Miyazaki², Yoshihiko Mizumoto¹, Junichi Morino², Kentaro Motohara⁸, Koji Murakawa², Masao Nakagiri⁴, Kyoto Nakamura⁷, Hidehiko Nakaya², Kyoji Nariai⁹, Tetsuo Nishimura², Kunio Noguchi¹, Takeshi Noguchi¹⁰, Junichi Noumaru², Ryusuke Ogasawara², Norio Ohshima⁷, Yoichi Ohyama², Kiichi Okita¹¹, Koji Omata², Masashi Otsubo², Shin Oya², Robert Potter², Yoshihiko Saito¹, Toshiyuki Sasaki², Shuji Sato¹², Dennis Scarla², Kiaina Schubert², Kazuhiro Sekiguchi², Maki Sekiguchi¹³, Ian Shelton¹⁴, Chris Simpson¹⁵, Hiroshi Suto², Akito Tajitsu², Hideki TAKAMI², Tadafumi TAKATA², Naruhisa TAKATO², Richard TAMAE², Motohide TAMURA¹. Wataru Tanaka¹⁶, Hiroshi Terada², Yasuo Torii¹, Fumihiko Uraguchi², Tomonori Usuda², Mark Weber², Tom Winegar², Masafumi Yagi¹, Toru Yamada ¹, Takuya Yamashita² Yasumasa Yamashita¹⁷, Naoki Yasuda¹, Michitoshi Yoshida¹¹, and Masami Yutani¹ Optical and Infrared Astronomy Division, National Astronomical Observatory, Mitaka, Tokyo 181-8588 iye@optik.mtk.nao.ac.jp²Subaru Telescope, National Astronomical Observatory, 650 North A'ohōkū Place, Hilo, HI 96720, USA ³National Astronomical Observatory, Mitaka, Tokyo 181-8588 ⁴Department of Astronomy, Graduate University for Advanced Studies, Hayama, Kanagawa 240-0193 ⁵ The Institute of Physical and Chemical Research (RIKEN), Wako, Saitama 351-0198 ⁶ Max-Plank für Astronomie, Königstuhl 17, 69117 Heidelberg, Germany ⁷Advanced Technology Center, National Astronomical Observatory, Mitaka, Tokyo 181-8588 ⁸Institute of Astronomy, School of Science, University of Tokyo, Mitaka, Tokyo 181-8588 ⁹Department of Physics, Meisei University, Hino, Tokyo 191-8506 ¹⁰ 290-2 Izawa, Misaki-cho, Isumi-gun, Chiba 299-4615 ¹¹Okayama Astrophysical Observatory, National Astronomical Observatory, Asakuchi-gun, Okayama 719-0232 ¹²Department of Astrophysics, Nagoya University, Chikusa-ku, Nagoya 464-8602 ¹³5-5-22-201 Sekimae, Musashino-shi, Tokyo 180-0014 ¹⁴David Dunlap Observatory, 123 Hillsview Drive, Richmond Hill, Ontario, L4C 1T3 Canada ¹⁵Department of Physics, Durham University, South Road, Durham. DH1 3LE, UK ¹⁶4-4-23 Takatanobaba, Shinjuku-ku, Tokyo 160-0075 ¹⁷ 1-14-12 Asahigaoka, Hino, Tokyo 191-0065

(Received 2003 October 9; accepted 2004 February 16)

Abstract

An overview of the current status of the 8.2 m Subaru Telescope constructed and operated at Mauna Kea, Hawaii, by the National Astronomical Observatory of Japan is presented. The basic design concept and the verified performance of the telescope system are described. Also given are the status of the instrument package offered to the astronomical community, the status of operation, and some of the future plans. The status of the telescope reported in a number of SPIE papers as of the summer of 2002 are incorporated with some updates included as of 2004 February. However, readers are encouraged to check the most updated status of the telescope through the home page, http://subarutelescope.org/index.html, and/or the direct contact with the observatory staff.

Key words: telescopes: instruments

1. History of the Project Planning and Construction

Conceptual planning for the 8.2 m (originally 7.5 m) Subaru Telescope began in the summer of 1984 when

2 M.Iye et al. [Vol. ,

an engineering working group was established by the Tokyo Astronomical Observatory of the University of Tokyo with full support from the optical and infrared astronomy community. In 1985 March, the Committee for Astronomy of the Science Council of Japan recommended the construction of the Japan National Large Telescope (JNLT) (Kodaira, Kogure 1986), the original name of the project that subsequently produced the Subaru Telescope, as the top priority amongst all other projects planned by the astronomical community. A Memorandum of Understanding between the Tokyo Astronomical Observatory and the University of Hawaii to sublease part of the summit area of Mauna Kea in Hawaii as a reserved site for the JNLT was signed in the summer of 1986. The first report summarizing the results of detailed studies was compiled in the "White Book" in 1986 September. In 1988 July, the Tokyo Astronomical Observatory was reorganized as an inter-university institute, the National Astronomical Observatory (NAOJ), to promote large-scale enterprises such as the JNLT project on a national basis (Kodaira 1989).

In 1989, active optics experiments were carried out for proof of concept (Iye 1989; Noguchi et al. 1989; Iye et al. 1990), and the effect of mirror seeing was quantitatively evaluated (Iye et al. 1991). At the same time, site tests were performed at Mauna Kea (Ando et al. 1989), and wind and water tunnel tests were carried out to identify the optimum shape of the enclosure (Ando et al. 1991).

A second advanced report, the "Blue Book", was compiled in 1989, in which most of the baseline features of the JNLT were presented, and the project was announced later that year at an international conference (Kodaira 1990). Acknowledging the dimensions and capabilities of the Keck Telescope and the Very Large Telescope of the European Southern Observatory, which began construction during the course of the 6-year feasibility study for JNLT, the target diameter of the primary mirror was expanded from 7.5 m to 8.2 m, without increase in the total budget.

Following the recommendations of the Science Council of Japan, the project was fully approved and construction of JNLT began in 1991 April (Kogure, Kodaira 1991). A call for proposals for renaming JNLT ended up with its new name, Subaru Telescope, after the old and familiar Japanese name for the visible star cluster Pleiades (Kodaira 1992). Progress of the project and the instrumentation plan was critically reviewed at another international conference held in Tokyo in 1994 (Iye, Nishimura 1995). The Subaru Telescope base facility was established at the University of Hawaii campus in Hilo, Hawaii, in 1997 April, and more than 20 NAOJ staff relocated from the Mitaka campus to begin work on the telescope in collaboration with local staff recruited through the Research Corporation of the University of Hawaii. The progress of construction was reported on several occasions (Iye 1997; Kaifu 1998), and the engineering First Light of the Subaru Telescope was achieved on 1998 December 24. Reports on First Light observations were published in 2000 (Kaifu et al. 2000; Iye et al. 2000). An inauguration Fig. 1. Concept of the active support system for the primary mirror.

Fig. 2. Structure of the mirror support actuator.

ceremony was held in 1999 September. The 9-year construction project was completed in 2000 March, and the telescope has been made available to both Japanese and the international community of astronomers since 2000 December.

2. Telescope Structure

2.1. Optics

The Subaru Telescope has an $8.2 \,\mathrm{m}\ F/1.83$ primary mirror with a focal length of 15 m. Three secondary mirrors are installed, each comprising a modified Ritchey–Cretien system at the F/12.2 Cassegrain or F/12.6 Nasmyth foci. The basic optical parameters are compiled in table 1.

The wide-field prime focus is the most notable feature of the Subaru Telescope, and is a unique capability among 8-10 m telescopes. An ambitious wide-field prime-focus corrector with a new type of atmospheric dispersion compensator (Nariai 1994) allows for a 30'field of view at F/2 with an optical image quality of better than 0''.23, right up to the edge of the field.

The Cassegrain focus offers a 6'field of view in combination with either the optical or infrared secondary mirror, depending on the instrument to be used. The optical Nasmyth focus utilizes a dedicated secondary mirror to cover a 4'field of view, and the infrared Cassegrain secondary can be used for observations at the infrared Nasmyth focus by moving the infrared secondary mirror along the optical axis and applying a force correction on the primary mirror shape. Although the coating and pupil size are different, the infrared secondary can be used for optical Nasmyth observations, and the optical secondary can be used for infrared Nasmyth observations, if necessary.

The infrared secondary mirror has chopping and tip-tilt correction capabilities, which are useful for near-infrared observations and indispensable for mid-infrared observations.

2.2. Active Mirror Support

Right from the beginning of the feasibility study, which began in 1984, fabrication of a light-weight mirror and the associated support system was identified as a critical issue. Finite element method (FEM) analyses were conducted to compare the deformation of the primary mirrors fabricated from honeycomb borosilicate glass and thin meniscus zero-expansion glass (Watanabe 1987). It became obvious that a conventional passive support would not provide the target image quality for such a large light-weight mirror, and a real-time force-controlled mirror support system to adjust for any surface shape error was consid-

Table 1. Parameters of optical components of the Subaru Telescope.

Mirror	Diameter	Radius of	Aspheric	Distance to
		curvature	constant	previous surface
	(mm)	(mm)		(mm)
M1(Primary)	8200	-30000	-1.008350515	_
M2(Opt/Cass)	1330	-5524.297	-1.917322232	-12652.174
M2(Opt/Nas)	1400	-5877.420	-1.865055214	-12484.300
M2(IR/Cass)	1265	-5524.297	-1.917322232	-12652.174

Table 2. Parameters of seven focal configurations.

Focus	Primary	Cass.	Nasmyth	Nasmyth	Cass.	Nasmyth	Nasmyth
wavelength	optical	optical	optical	optical	infrared	infrared	infrared
Image derotation	Instr. Rot.	Instr. Rot.	Ima. Rot.	None	Instr.Rot.	Ima. Rot.	None
Ritchey-Cretien	NA	Yes	Yes	No	Yes	No	No
Focal length (mm)	15000	100000	104207.0	102244.5	100000	108512.4	110605.2
Pupil diameter (mm)	8200	8200	8200	8200	8081.9	7971.6	7947.5
Back focus (mm)	NA	3000	4992.6	4600	3000	4600	4992.6
Effective F ratio	1.83	12.195	12.708	12.469	12.373	13.612	13.917
Field of view (arcmin)	30	6	3.5	6	6	3.5	6
Field curvature (mm)	NA	5630.3	6108.5	6106.6	5630.3	5635.2	5636.3
Plate scale	13.75099	2.062658	1.979385	2.017378	2.062658	1.900850	1.864884

ered to be mandatory. In light of this, borosilicate glass, which has a thermal expansion coefficient more than 100times higher than that of thin meniscus glass, became less desirable in terms of the stringent thermal control required for the massive primary mirror. The study group also judged that force control, though not an easy approach, is more tractable than temperature control. As the approach to use and control segmented mirrors, rather than a monolithic mirror, did not appear to be feasible at the time of decision making, monolithic, thin meniscus zero-expansion glass was adopted for the primary mirror. Following FEM studies of the support system, a support system consisting of 261 actuators distributed in 8 rings was adopted to support the mirror. The mechanism of support, itself, is also unusual in that instead of supporting the mirror using supports mounted orthogonally on the back surface, which is an edge-moment support that induces sigmoidal deformation of the tilted mirror, the actuators are inserted into "pockets" bored into the back of the blank at the 261 actuator locations (cf. figure 1). This configuration effectively supports the glass mirror at local centers of gravity, avoiding any sigmoidal deformation and significantly reducing the overall bending. The decision to proceed with this challenging design was difficult, because the thinness of the mirror blank and the many pockets that needed to be drilled from the back greatly increased the potential risk of breaking the glass. However, the study team decided to control the risk by carefully designing the production processes and the supporting structure considering the higher imaging performance expected from this concept.

The actuator mechanism for this mirror support system is shown in figure 2. The support force is applied by a spring on a ball screw, and the force is measured by a

Fig. 3. Surface error map for the $8.2~\mathrm{m}$ primary mirror as shown in 20nm interval contour map.

precise force sensor based on a tuning-fork quartz oscillator. The sensor was designed to achieve a 10^{-5} resolution and a dynamic range of 0–1500 N. The temperature coefficient is measured and calibrated for each actuator. In this configuration, both the axial and lateral support forces are applied at the local center of gravity of the blank. Lateral support is accomplished passively with a counterweight.

2.3. Fabrication of the Primary Mirror

The primary mirror blank, 8.3 m in diameter and 30 cm in thickness, was manufactured using Ultra Low Expansion (ULE) glass by Corning Incorporated, Canton, New York. To ensure the quality of the final mirror, the monolithic blank was fabricated from 44 hexagonal ULE blocks with thermal expansion coefficients in the range ± 5 ppb, manufactured over the first two years. Some of the hexagonal blocks were cut further into two or three pieces to give a total of 55 pieces to form a circular disk, and were then arranged and thermally fused in a heating furnace to form the 8.3 m monolithic blank. The pieces were arranged according to annealing simulations based on their expansion coefficients so as to minimize the residual surface error and in consideration of active correction for thermal deformation (Mikami et al. 1992). The optimum solution, in fact, provided a residual surface error that was an order of magnitude smaller than that given by the random solutions. Thermal fusion of the pieces into a monolithic structure was completed early in 1994. After grinding the front surface, the blank was turned over to grind the back surface. Finally, the blank was

Fig. 4. Schematic of telescope structure.

slumped over a spherical mold in a heating furnace to an approximate meniscus shape so as to reduce the amount of grinding work required (Sasaki et al. 1994).

The thin meniscus mirror blank was then transported in the summer of 1994 to Contraves Brashear Corporation near Pittsburgh for polishing. The first operation was to bore 261 pockets on the back surface of the blank for inserting the invar sleeves to support the mirror. Each pocket was 15 cm deep by 15 cm in diameter. The drilled surface was then polished and acid-etched to remove any remaining micro cracks on the surface. The mirror blank was again turned over in the autumn of 1995 for processing of the front surface. Grinding and polishing was carried out in a 36 m-high underground shaft constructed at the large optics facility of Contraves Brashear Corporation, Wampum, near Pittsburgh. This stable underground facility has advantages over the conventional tower facility, avoiding vibrations induced by wind load and traffic, as well as diurnal tilt of the shaft induced by the thermal load of the sunshine to the tower.

The primary mirror was set on a rotating polishing bed with 261 hydraulic supports distributed identically to the actual active support system. The polishing procedure was executed using a computer-controlled polishing machine, ensuring careful maneuvering of the work functions. The progress of polishing was monitored by various independent measurements, including profilometer, infrared interferometer, optical interferometer, and penta prism measurements.

The finished mirror has a physical diameter of 8.3 m, a thickness of 20 cm and a weight of 22.8 tonnes. The diameter of the effective reflecting surface is 8.2 m, and the focal length is 15 m. The final surface error after compensating for the first 21 modes of deformation by the active optics system was demonstrated to be 14 nm rms on 1998 August 28. The surface error map is shown in figure 3.

2.4. Telescope Structure

On the alt-azimuth mount structure, the entire telescope is 22.2 m in height and 27.2 m wide, with a moving assembly weighing 555 tonnes (figure 4). The telescope can be driven at a maximum slew rate of $0.^{\circ}5/s$, and the cable wrap allows for rotation of 270° in each direction from the south. The top ring and the mirror cell are supported from the center section by trusses to ensure minimum flexure and to maintain the optical alignment between the primary and secondary mirrors. The secondary mirror unit is suspended by a torsion-resistant spider with a special locking mechanism to secure the secondary mirror units or primary focus unit into the inner ring supported by the spider (Miyawaki et al. 1994).

The tertiary mirror tower houses two tertiary mirrors, one for the optical Nasmyth and the other for the infrared Nasmyth foci. These tertiary mirrors can be inserted and

Fig. 5. Water tunnel test showing the stream lines around the enclosure.

Fig. 6. Subaru enclosure vertical layout.

removed in about 12 minutes. The primary mirror cover consists of 23 separate panels suspended by wires from the center section and 4 side covers that can be opened or closed in about 7 minutes when the telescope is pointing to the zenith.

The mirror cell houses 261 actuators to support the primary mirror. There are three additional fixed point devices with a mechanical fuse mechanism to avoid the accumulation of excess force at these fixed points. The mechanical fuses are triggered (released) to protect the mirror when the force applied at the fixed points exceeds a threshold value, 1.5 tonnes, as may occur during an earthquake, for example. In the initial phase of operation, the metal pad fixed to the primary mirror for this purpose became unstuck on a few occasions, attributed to imperfect adhesion. New pads were designed and replaced in the summer of 2001 to ensure functionality in the event of larger forces at the adhering surface. The mechanical fuse was also readjusted to function at a lower level of 0.5 tonnes force to ensure the safety of the primary mirror.

An acquisition and guide system consisting of a Shack–Hartmann camera, a guider unit, and a calibration lamp unit is installed at each operating focus. The Cassegrain unit also houses the adaptive optics system, located in front of the acquisition and guiding system. A hydrostatic bearing system, driven by a direct-drive linear motor, ensures very smooth pointing and tracking operation.

Actual fabrication and pre-assembly of the telescope structure was completed in Osaka in 1996 (Noguchi et al. 1998), and the disassembled parts were shipped to Hawaii for reassembling at the summit, which began in 1996 October. Installation of the telescope structure in the enclosure was completed in 1998 without incident. The actual performance of the telescope is discussed later.

2.5. Enclosure and Support Facilities

A series of studies was conducted to compare the aerodynamic performance of the enclosure with the traditional hemi-spherical shape, cylindrical shape and others (Mikami et al. 1989; Ando et al. 1991; Mikami et al. 1994). It was found that a cylindrical enclosure is superior to a hemi-spherical dome in terms of preventing the turbulent surface boundary layer from advancing up along the enclosure and deteriorating the observation conditions (figure 5). In order to ensure smooth flow of flushing air to carry away any residual warm air near the telescope environment, two huge walls, named "The Great Wall", were constructed, along with a number of ventilators and

Fig. 7. Aerial view of the Subaru enclosure.

Fig. 8. Top unit handling system.

Fig. 9. Layout of the coating facilities and mirror handling equipment on the ground floor of the enclosure.

louvers to control the air flow inside the enclosure.

The Subaru site was chosen at a latitude of 19°49′43″N, longitude of 155°28′50″W, and altitude of 4139 m (Ando et al. 1989). The construction of the lower part of the enclosure building began on 1992 July 6. The ground cinder soil of the site was first stiffened by adding huge amount of cement and water. A robust concrete foundation was laid to support the 2000 tonnes of the enclosure, and the telescope pier, 29 m in diameter and 14 m high, was then erected, followed by the construction of the steel reinforced concrete building of the lower part of the enclosure.

Construction of the upper part of the enclosure, which corotates with the telescope, was initiated in the summer of 1994. The entire structure was built on the azimuth rail at the top of the lower building. The enclosure has five floors; the observation floor, Nasmyth floor, tertiary floor, top unit floor, and top crane floor (figure 6). The outer wall is covered with aluminum panels, and the structure has an overall height of 43 m and a base diameter of 40 m (figure 7). The aluminum outer panel reflects the blue sky and appears less conspicuous than conventional white painted domes. Also, the aluminum panel has lower emissivity than the white painted domes and does not cool down excessively during the night. It is beneficial for reducing the temperature difference between the enclosure and the ambient air.

All the secondary mirror units and the prime focus unit are housed in a carousel on the top-unit floor. Exchanging these top units is achieved by manipulating the top unit handling system (Kurakami et al. 2003), and takes 3 to 6 hours (figure 8).

2.6. Mirror Coating Facilities

The mirror handling facility, mirror washing facility, mirror cell trolley, and mirror coating chamber are located on the basement floor of the enclosure (figure 9). Realuminizing the primary mirror requires the telescope to be non-operational for a minimum of two weeks. The first step in the realuminization operation is to lift the mirror cell trolley from the ground floor to the observation floor through the 10 m mirror hatch using the 80 tonne top crane. The mirror cell trolley then accepts the mirror cell from the telescope. The top crane lowers the mirror cell with the primary mirror down to the ground floor, where the primary mirror is detached from the mirror cell using a hoist. After being transferred to the lower cell of the mirror vacuum chamber, the mirror is moved in underneath the mirror washing facility. The mirror is washed and then sprayed with hydrochloric acid to remove any existing aluminum film. All the chemicals and waste

water used to this operation is gathered and disposed in accordance with the local regulation. Several steps follow washing and drying the surface. Finally, the lower cell is moved to underneath the upper cell of the vacuum coating facility (Yutani et al. 2003).

The vacuum-coating chamber contains aluminum filaments for the evaporative coating of aluminum (Hayashi et al. 1998). Due to power limitations, aluminum deposition is performed by firing the filaments in three grouped zones. The measured reflectivity of the aluminized witness sample verifies that the reflectivity exceeds 91% at 500 nm (Kamata et al. 2003).

2.7. Control System and Data Archive System

Figure 10 shows the configuration of the computer systems at the summit, Hilo base facility, and the Mitaka campus. A dedicated optical-fiber link connects the summit to the Hilo base facility, and the Hilo base facility to the Mitaka campus to ensure swift transfer and backup of observation data. Remote monitoring and remote operation of the telescope has been tested, and a range of observations can be performed by linking the summit either to Hilo base or to Mitaka.

Figure 11 illustrates the overall architecture of the observation control system for the Subaru Telescope. The kernel of the telescope control (TSC) system is a TSC server linked to three user interfacing workstations, TWS1-3. This system controls the mid-level processors. MLP1-3. MLP1 controls all of the driving function of the telescope, enclosure, instrument rotators, image rotators, atmospheric dispersion correctors, and other peripheral optics devices. MLP2 handles the active support system of the primary mirror, and MLP3 monitors and controls the telescope environment. Actual control of each component is carried out by dedicated board computers, called local control units (LCUs). All of these computers are linked by local-area networks (Ogasawara et al. 1998; Sasaki et al. 1998; Kosugi et al. 1998; Noumaru et al. 1998; Tanaka et al. 1998). Control of observations is supervised by the supervisor workstation (OBS). Observers can send commands from observation operation terminals OWS1-3 to OBS. The observational instruments are controlled by the instrument control computer (OBCP), which is interfaced to OBS and the data-acquisition system (OBC).

A huge data archive system with 600 TB of tape storage capacity and a supercomputer are installed to cater for high-load data analyses, simulations, and weather forecast of Mauna Kea (Ogasawara et al. 2002a; Ogasawara et al. 2002b). The entire software system consists of three packages; the Subaru Observation Software System (SOSS) (Sasaki et al. 1998), the Subaru Telescope data Archive System (STARS) (Ogasawara et al. 1998; Takata et al. 2000), and the Distributed Analysis System Hierarchy (DASH) (Mizumoto et al. 2000; Yagi et al. 2003; Ogasawara 2002c). Figure 12 shows the configuration of these systems at the Hawaii and Mitaka campuses.

6 M.Iye et al. [Vol.,

Fig. 10. Subaru computer network linking the summit, Hilo base, and Mitaka.

Fig. 11. Subaru observation control system architecture. (Right) Telescope control system, (left) observation control system, (upper) workstations used as user interfaces, (middle) control servers, and (bottom) hardware control systems.

Fig. 13. Available open-use instruments for the Subaru Telescope.

Fig. 14. Observational capability of open-use instruments.

3. Common-Use Instrument Suite

The Subaru observational instruments plan and its status have been reported in several papers (Iye, Nishimura 1995; Iye, Yamashita 2000; Yamashita, Nishimura 2003). The entire Subaru instrument suite consists of 7 instruments: 1) Subaru prime-focus camera (Suprime-Cam), 2) Faint Object Camera And Spectrograph (FOCAS), 3) High-Dispersion Spectrograph (HDS), 4) InfraRed Camera and Spectrograph (IRCS), 5) OH airglow Suppression spectrograph (OHS), 6) COoled Mid-Infrared Camera and Spectrograph (COMICS), and 7) Coronagraphic Imager with Adaptive Optics (CIAO). These instruments are deployed at the prime focus (Suprime-Cam), optical Nasmyth focus (HDS), infrared Nasmyth focus (OHS), and Cassegrain focus (FOCAS, IRCS, COMICS, and CIAO) as shown in figure 13.

Figure 14 shows the region in the wavelength–spectral resolution plane covered by these instruments. Table 3 is an updated summary of the key parameters of these instruments. All of the instruments employ closed-cycle refrigerators to cool the detector and/or the instrument, and liquid nitrogen is not used for the CCDs.

3.1. Suprime-Cam

Suprime-Cam, covering a $34' \times 27'$ field of view with an unvignetted area of 30' diameter, by ten $4k \times 2k$ CCDs, is the most frequently used Subaru Telescope instrument. The wide field, high quality, prime focus corrector provides superb image quality as good as 0."3 even near the edge of the field under a good seeing condition. The median seeing size in the $I_{\rm C}$ -band is 0."61 and the mean of the median seeing size in all the bands is 0."69. The stellar images are round and the mean ellipticity of the point sources is $2.3 \pm 1.5\%$. Standard sets of broad band filters $B, V, R_{\rm C}, I_{\rm C}, g', r', i'$, and z' and a number of narrow band filters are available with some restriction on usage. Suprime-Cam has an automatic filter exchanger that can hold up to 10 filters. Upgrading the readout electronics to Messia V enabled fast readout within 53 sec to increase the observing efficiency (Miyazaki et al. 1998; Komiyama et al. 2003; Miyazaki et al. 2002).

3.2. FOCAS

The FOCAS is a Cassegrain instrument with high-throughput all-refractive optics optimized for a wavelength region of 365-900 nm. The instrument has an unvignetted field of view of 6'at 0.''1/pixel sampling with two buttable $4k \times 2k$ pixel CCDs mounted with a butting separation of less than $100\mu m$. The FOCAS has a direct imaging mode, a long-slit spectrographic mode, a multi-slit spectrographic mode, and a polarimetric imaging and spectroscopic mode. A spectral resolution of R=250-2000 is available for a slit width of 0.''4 by selecting one of the 4 grisms. High-dispersion grisms and an echelle grism are under verification tests and will become available soon (Kashikawa et al. 2000; Yoshida et al. 2000; Kashikawa et al. 2003; Kawabata et al. 2003; Saito et al. 2003).

3.3. HDS

The HDS is a Nasmyth echelle spectrograph with a quasi-Littrow configuration (Noguchi et al. 2002). A catadioptric camera with a triplet corrector is used to allow covering a wide wavelength region of $0.3-2.3\mu\mathrm{m}$. However, only optical CCDs are provided as the detector. An echelle grating with 31.6 gr mm⁻¹ blazed at 71.°5 is used as the primary disperser. Two cross-disperser gratings, optimized for the blue and red regions, are also installed, and one is selected to obtain the optimum order separations on the CCDs. The HDS is designed to provide a spectral resolution of R=100000 with a 0."4-wide slit, which projects onto $45\mu\mathrm{m}$, or 3 pixels, of the CCD.

3.4. IRCS

The IRCS is a common-use instrument for near-infrared (1-5 μ m) imaging and spectroscopy at diffraction-limited spatial resolution. The instrument was constructed at the Institute for Astronomy of the University of Hawaii. An echelle spectroscopy mode is provided in addition to the imaging mode and the grism spectroscopy mode (Kobayashi et al. 2000; Terada et al. 2003).

3.5. OHS

The OHS is an original instrument designed and constructed at Kyoto University (Maihara et al. 1993). The instrument has a first-stage medium resolution ($R \sim 5000$) spectrograph that produces an infrared spectrum on a reflecting mirror with a specially designed mask to remove OH airglow lines. The reflected light, free of OH features, is contracted into white light and fed into a low-resolution spectrograph/camera to produce a near-infrared spectrum for very faint objects (Iwamuro et al. 2001). The spectro-

Fig. 12. Distributed data archive systems for the Subaru Telescope.

Table 3.	Parameters	$\circ f$	common-use	instruments.

Instrument	Focus	Modes of	Spectral	Spectral	FOV	Pixel
		observation	coverage	resolution		scale
Suprime-Cam	Prime	Im	B, V, R, I, z, NBF	10-100	$34' \times 27'$	0."2
FOCAS	Cass	Im/MOS	$0.36 - 0.90 \ \mu \mathrm{m}$	10 - 2000	$6'\phi$	0."1
HDS	Nas	Sp	$0.3 - 1.0 \mu m$	100000	$10'' \times 0.''4$	0."13
IRCS	Cass	Im/Sp	$1.0 - 5.4 \ \mu { m m}$	10 - 20000	$1' \times 1'$	0."023/0."075
OHS/CISCO	Nas	Im/Sp	J,H,K	10 - 800	$2' \times 2'$	0."12
CIAO	Cass	Im/Sp	z,J,H,K,L',M'	10 - 600	$22'' \times 22''$	0."012/0."022
COMICS	Cass	Im/Sp	N,Q	10 - 10000	$42'' \times 31''$	0."13/0."165

graph/camera module of this instrument, CISCO (Cooled Infrared Spectrograph and Camera for OHS), can be used separately as an imaging device at the Nasmyth focus (Motohara et al. 2002).

3.6. CIAO

The CIAO is an instrument dedicated for diffraction-limited imaging of faint objects around a bright point source, such as circumstellar disks, circumstellar envelopes of evolved stars, and quasar host galaxies. It has a set of occulting masks as small as 0."1 in diameter to allow imaging of structures very near the central source, utilizing the infrared adaptive optics system. The system provides both grism spectroscopic and polarimetric observational capabilities (Tamura et al. 2000). The instrument has been commissioned, and the status of the instrument is described in Tamura et al. (2000); Tamura et al. (2003); Murakawa et al. (2003).

3.7. COMICS

The COMICS is an instrument housing 6 arrays of 320×240 Si:As IBC detectors for the 8–13 and 16–26 μm bands. It has an imaging capability of 0″.13 /pixel, covering a field of dimensions $42'' \times 31''$. Long-slit spectroscopy covering up to 40''at 0″.165/pixel resolution is also available. The readout electronics newly developed for COMICS enabled this instrument to be the first mid infrared instrument with new-generation array offered for open use on 8m class telescopes (Kataza et al. 2000; Okamoto et al. 2003; Sako et al. 2003).

3.8. Adaptive Optics

The Cassegrain adaptive optics (AO) is optimized for use in the K band (Takami et al. 2003a; Takami et al. 2003b). IRCS and CIAO are designed to use this AO system. A bimorph deformable mirror driven by 36 electrodes is used to compensate for any wavefront aberration as measured by a curvature wavefront sensor with 36 avalanche photodiodes operated in the photon-counting mode. The wavefront sensing beam is divided and directed to the 36 photodiodes through a custom-designed microlens array, so as to match the distribution of electrodes on the bimorph mirror. An oscillating membrane

is used to generate the necessary offsets of the pupil image immediately in front and behind the detector array. The wavefront sensor is mounted directly on the instrument so as to minimize the relative flexure between the wavefront sensor and the instrument. The unvignetted field of view of the AO system is 120"in diameter. The current AO system provides, with a guide star brighter than $R_{\rm C}=13$ mag, corrected images of 0".065 in FWHM with a Strehl ratio of 0.4 in the K band within a field of 20" in diameter. By inserting the retractable feed mirror in front of the Cassegrain focal plane, an observation can be switched easily between the ordinary mode and the AO mode without changing the focal position of the instruments or the F ratio of the incident beam. The total bandwidth is about 100 Hz. Usage of a laser guide star is expected in 2005 to increase the sky coverage for AO (Hayano et al. 2000; Hayano et al. 2003).

4. Operation Performances

Although the Cassegrain first light was achieved at the end of 1998, commissioning all four foci and seven common-use scientific instruments took another two years. Limited open use of the Subaru Telescope was offered from 2000 December. For the first semester S00B, from 2000 December to 2001 March, only Suprime-Cam and CISCO were available. However, other instruments gradually became available, firstly with limited modes of operation, but eventually with all modes of observation planned for each instrument. Although the failure rates are gradually being reduced, further improvements are required to reach stable and efficient operation of the telescope and instruments.

The telescope was closed for two months from 2001 August to September to address the problem of detached pads on the back of the primary mirror incorporated as part of the mechanical fuse system. The mirror was realuminized during this period and in 2003 August.

4.1. Active Mirror Support

A block diagram of the active support system for the primary mirror is shown in figure 15. The control system consists of two feedback loops. The main servo con-

Fig. 15. Block diagram of the active support system for the 8.2 m primary mirror.

Fig. 16. Dynamic performance of the residual surface error of the mirror as derived by contiguous Shack-Hartmann measurements

Fig. 17. Seeing size statistics. The diamonds, squares, and circles indicate the measurement time before 21:00, 21:00–26:00, and after 26:00 Hawaiian standard time, respectively.

trol of the support force loop is activated every 100 ms according to an open-loop force command issued by the real-time control computer. The computer updates the support force for the current elevation angle of the telescope based on a series of functions calibrated by mirror analysis, which is carried out when the focal configuration is changed. The mirror analysis is performed using a Shack-Hartmann camera installed at each focus. The displacement of 136 spot images of a bright star, produced by an array of microlenses with 14×14 subapertures, are measured to derive the surface error of the primary mirror. An exposure time of 60 s is adopted to achieve a wavefront measurement accuracy of 28 nm rms by averaging out atmospheric turbulence. The surface error is expanded by the eigenmodes of the primary mirror, and the coefficients of the first 32 eigenmodes are used to derive the optimum correction force to be added for each of the 261 actuators. Calibration of the active support system is established by performing such measurements at various orientations.

The actual dynamic performance of the mirror surface is measured by repeating the Shack–Hartmann wavefront measurements for 1 hour. Figure 16 shows an example of such measurements carried out during 12:15–13:15 UT on 2001 September 27 at elevation angle $50^{\circ}-46^{\circ}$. The surface error on average is about 200 nm rms (Takato et al. 2003). The current rms surface error of the primary mirror is about 300-400 nm, which corresponds to an image spread of 0.15-0.12 at all elevation angles ($\sim 20^{\circ}$ to 85°). Under the best conditions, error of less than 100 nm has been achieved.

There are three measures that can be taken to improve the residual surface error of the primary mirror: (1) The support force distribution can be fine tuned by taking the thermal-deformation effect of the primary mirror and the mirror cell into account in more detail. (2) A real-time feed back loop using light from an offset guide star directed to the Shack—Hartmann camera by a dichroic prism can be implemented. (3) A real-time fixed-point feedback (FFB) system can be introduced to reduce the wind load on the three fixed points (Kanzawa et al. 2003).

Fig. 18. Monthly average seeing size during the 2000 June – 2002 December period.

Fig. 19. Wind screen and wind sensors.

Fig. 20. Mirror temperature with respect to the ambient air temperature.

4.2. Image Quality

The full width at half maximum (FWHM) seeing size measured by the CCD camera of the auto guider in the red band during focus checks has been recorded since 1999. Figure 17 shows the seeing size statistics for the period 2000 May to 2002 July. The median image size is 0.%6-0.%7 FWHM in the $R_{\rm C}$ and $I_{\rm C}$ bands at all four foci. The best images obtained so far are 0.%2 FWHM without AO and 0.%065 with AO in the near-IR K-band, and 0.%3 in the optical and mid-IR. This figure also shows that the seeing is generally slightly better at the later half of the night, probably due to better thermal equilibrium achieved with the ambient air.

Figure 18 shows the monthly average seeing size in arcsec as measured during the 2000 June – 2002 December period. There is a repeated seasonal trend of seeing variation. The best average seeing of 0.5 is achieved during September, and May is the second-best month.

The temperature of the primary mirror and the enclosure are controlled during the day to a few degrees below the predicted night-time temperature so as to reduce the facility seeing. Approximately during a one-hour prior to the start of evening observation, all of the ventilators are opened to let air flow in the enclosure, thus assisting to reduce the temperature difference between the structure and the ambient air (cf. figure 19). Figure 20 shows the measured temperature difference between the primary mirror and the ambient air. The details of the temperature control and the seeing statistics have been reported by Miyashita et al. (2003).

Fig. 21. Az track levels undulation as measured in 1997 January and in 2002 February. The unevenness increased from 0.1 mm to 0.3 mm p-p, probably due to a persistent uneven load distribution. A fine tuning of the rail to reduce this undulation is foreseen.

4.3. Pointing Performance

The telescope can be pointed for elevation angles of $89^{\circ} \geq El \geq 15^{\circ}$. However, to avoid any fast movement of the telescope near to the zenith, and large extinction at lower elevation angles, planning of an observation in the elevation angle range $85^{\circ} \geq El \geq 30^{\circ}$ is recommended. The blind pointing accuracy is better than 1."0 rms across most of the sky. The 30"field of view of the acquisition guide camera with a 0."07 positioning accuracy is sufficient for

Fig. 22. Control block diagram for the IR secondary mirror.

all imaging observations. For spectroscopic observations, short acquisition images should be taken to ensure that the target remains on the center of the spectroscopic slit width.

The parameters of the telescope pointing model equation are calibrated whenever the top unit is changed. The high-precision repeatability of the top unit exchange operation is proved by the stability in the offset values of the pointing model. Small systematic changes in some of the parameters were observed after aluminum re-coating and repairs on the fixed-points pads during the summer of 2001.

4.4. Tracking Accuracy

The Subaru Telescope runs on a circular azimuthal track rail. Six hydrostatic oil pads lift the 555 tonne telescope by about 50 μ m, and six linear magnetic motors drive the telescope directly without any stick-slip. Due to the small discontinuity in the level of adjacent track rails, the tracking fails by as much as \sim 2"when the pad passes these joints. Software correction using a lookup table was applied to address this problem (Tanaka et al. 1998), with the result that an open-loop tracking error of less than 0."2 rms for 10 minutes has been achieved. Non-sidereal tracking of the telescope using a look-up table is also feasible. The tracking error has reportedly increased over the last two years, and is currently being investigated.

Azimuthal track rails were installed in 1997 January with a peak-to-peak leveling error of 0.1 mm. In 2002 February, the vertical undulation of the azimuthal rails was found to have increased to 0.3 mm, attributed to uneven sinking of the non-shrink mortar underneath the azimuthal track rails. Figure 21 shows the increase of the measured undulation of the track rail as a function of the telescope pointing (Usuda et al. 2003). A newly implemented Az correction table has restored the open-loop tracking accuracy.

4.5. Performances of Acquisition Guide System

The measured guiding error, including the seeing effect, is less than 0.11 rms with a guide star brighter than magnitude 16. The readout noise of the acquisition/guide camera at the Cassegrain and prime foci is $\sim 10 \, \mathrm{e}^{-1}$, while that at the Nasmyth foci is as high as $100 \, \mathrm{e}^{-1}$. The acquisition time has been shortened to less than 1-2s.

4.6. Infrared Secondary Mirror

The tip-tilt and chopping infrared secondary mirror (Itoh et al. 1998) is made of light-weight ULE glass (185 kg) and has a silver coating. Figure 22 shows the control block diagram for the IR secondary mirror. The driving mechanism consists of 6 electro-magnetic actuators, 15 bellows for passive support, 3 electric capacitance sensors, and a reaction force compensator. The maximum chopping frequency currently available is 3 Hz with a duty cycle

of 80% and a position error of < 0.11 rms. The chopping amplitude is 60, and the sampling rate and detection rate of the sensors are both 1 ms.

The rms residual guiding error with the tip-tilt secondary mirror was measured to be 0.028 using the fast guiding system with a guide star of magnitude 11–14.

Fig. 23. Binary star image taken using the FOCAS instrument on 2000 August 9. The upper star is a red star, and the lower is a blue star. The image of the blue star is clearly elongated when the ADC is not at correct rotation angle. The seeing was about $\sim 0.^{\prime\prime}6$.

Fig. 24. Reflectivity and surface roughness degradation of the primary mirror measured at 670 nm.

4.7. Atmospheric Dispersion Correction and Image Derotation

The atmospheric dispersion corrector (ADC) units, comprising a counter-rotating pair of direct-vision prisms with matching silicon oil, are installed at the Cassegrain and Nasmyth foci to compensate for atmospheric dispersion down to an elevation angle of 30°. The ADC for the prime focus is based on different optics (Nariai 1994) and is assembled in the top unit module for the Suprime-Cam. Figure 23 shows test images for a pair of blue and red stars taken using the FOCAS (Kashikawa et al. 2003) at an elevation of 55° with the ADC at various settings. The image of the blue star is clearly elongated when the ADC is not at the correct rotation angle.

The instrument rotators for field derotation are installed at the prime focus and Cassegrain focus, while three-mirror image derotators are equipped at Nasmyth-Opt and Nasmyth-IR foci. The derotation error at the prime focus and Cassegrain focus is practically negligible. The derotation error at the Nasmyth foci is less than $< 0.^{\circ}02hr^{-1}$.

4.8. Reflectivity of the Primary Mirror

The latest realuminization of the 8.3 m primary mirror was conducted in 2003 August. It was the fourth such maintenance operation conducted since the arrival of the mirror at the summit in 1998. As a maintenance routine, the mirror is cleaned with CO_2 dry ice every 2 to 3 weeks under lower (50%) humidity conditions using an in situ cleaning device consisting of 4 deployable arms mounted at the lower edge of the center section. These arms are fitted with many nozzles to supply dry ice to the mirror surface, and are swept over the entire mirror surface to remove dust accumulated on the mirror surface (Torii et al. 1998). Figure 24 shows how the reflectivity of the primary mirror decreases over time. At optical wavelengths

 $(\lambda = 670 \text{ nm})$, the reflectivity is kept better than 82-83% and the surface roughness is 70-80Å as measured using a scatter meter (μ Scan, TMA Technologies, Inc.).

Fig. 25. CIAX cart for Cassegrain instrument exchange operation dismounts an instrument from the Cassegrain focus and brings it to one of the four Cassegrain instrument standby ports. CIAX then takes the next instrument from the standby port and mounts it back to the Cassegrain focus.

Fig. 26. Two of the four Cassegrain instruments standby ports. FOCAS is mounted on one of the ports, but the other port for IRCS is unoccupied in this picture.

4.9. Instrument Exchange

Exchange of the Cassegrain instruments is achieved effectively and smoothly with using the Cassegrain Instrument Automatic eXchanging system (Usuda et al. 2000). Figure 25 shows the CIAX cart carrying one of the Cassegrain instruments, CIAO, during the exchange operation. This can be performed during the day, and takes about two hours. There are four stand-by platform ports on the Cassegrain floor where the remaining three instruments can be kept alive with an electric and cryogenic power supply as well as connection to the network system. Figure 26 shows two such stations where one of the stations is occupied by FOCAS.

Exchanging the top unit requires 3–6 hr of work during the day. Linking and resetting the secondary mirror requires an additional 30 min. Inserting the tertiary mirror takes only 2 min. Rotation of the enclosure takes less than 6 min. Although the level of operation of the telescope and instruments have become smoother and more stable over the last two years, there are still, naturally, many areas where improvements can be made to increase operational efficiency.

During the 28 months between 2000 May and 2002 August, the telescope was operational for 26 months. The top unit was exchanged 56 times and the instruments were changed 89 times, corresponding to roughly 2.2 top unit exchange operations and 3.4 instrument exchange operations per month.

4.10. Efficiency of Operation

Software revisions were made to reduce the time required for pointing the telescope by improving the control

Fig. 27. Increase of science exposure time fraction in Suprime-Cam observations. "Readout + Calib" is the time fraction for calibration exposures and CCD readouts for both science frames and calibration frames. "Others" include time for telescope pointing, setting up for a guide star, filter exchange, and other preparatory works. It must be noted that telescope idling time waiting for expectant improvement of poor weather condition is also included in "Other".

Fig. 28. Nights assigned for open-use programs in five categories of science observation.

Fig. 29. Numbers of assigned nights for open-use programs requesting each of the open-use instrument. Because the Adaptive Optics is usually used either with IRCS or with CIAO, those nights are doubly counted on each instrument.

parameters and algorithm. Also made were modifications of the drive mechanisms and the procedure to speed up the top unit exchange and Cassegrain instrument exchanges. Together with these efforts to improve the operation efficiency of the telescope, separate efforts on instruments have been made during the last few years.

Figure 27 shows the fraction of science exposure time for Suprime-Cam observations during the time when the telescope dome was open (Noumaru 2002). The minimum overhead between successive CCD exposures used to be about 240 s for the Suprime-Cam, which includes CCD wipe out and the signal readout. The overhead became shortened to 120s by replacing SITe CCDs to MIT/LL CCDs in 2001 April, and was reduced eventually to 60s by virtue of newly developed readout electronics; Messia-V (Komiyama et al. 2003). One can read in this figure the tendency of improved shutter open time fraction in accordance with these improvements. The actual fraction of time spent on target exposure measured versus the time with the telescope pointed to the target was of course even larger and is now about 75%, depending on the filters and the observed objects.

4.11. Open-Use Statistics

The Subaru Telescope was made available for open use in 2000 December (S00B semester), with only Suprime-Cam and CISCO offered to the community. Now, all seven open-use instruments and the Cassegrain adaptive optics system are available for open use. Some of the instruments, however, are offered with some operational restrictions. All applications for open-use time are reviewed by referees nominated by the Time Allocation Committee (TAC), and the TAC prepares a list of successful proposals. The competition rate over the last seven semesters has on average been 5 times for proposals and 6 times for nights. Table 4 gives the statistics for open-use applications. In order to increase the opportunity for potential users to obtain observing experience using the Subaru Telescope, TAC decided to accept only short programs requiring no more than 3 nights for the first three semesters. However, from semester S02A, larger scale programs with a maximum of 10 nights have been considered to derive science outcomes on systematic studies. Figure 28 shows the number of assigned open-use nights in five major fields for semesters S00B-S03B, and figure 29 shows the number of assigned open-use nights for individual instruments for semesters S00B-S03B.

In addition to these open-use programs, two major coordinated projects, the Subaru Deep Field Survey (SDF),

C ,	0.1 1	A 1 / 1	D / 1	A · 1
Semester	Submitted	Adopted	Requested	Assigned
	proposals	proposals	nights	$_{ m nights}$
S00B	114	26	223	36
S01A	105	27	204	36
S01B	160	29	337	47
S02A	186	37	410	69
S02B	193	38	448	74

40

45

Table 4. Statistics on open-use application.

the Subaru–XMM Deep Field Survey (SXDS), and the Subaru Disk and Planet Search (SDPS) have been organized and are conducted by the observatory staff, for which up to 33 nights per year in total have been dedicated until S03B.

S03A

S03B

195

196

Science outputs from Subaru Telescope are published in many papers. Short reviews on some of the scientific achievements are made (Iye 2003).

5. Future Plan

Second-generation instruments, FMOS and MOIRCS, are currently under construction. FMOS is a fiber multiobject spectrograph for the J and H bands to be mounted at the prime focus for spectroscopic observation of up to 400 objects in a 30' field (Maihara et al. 2000). Two sets of Echidna, each having 200 fiber head positioners installed in the focal plane unit, pick up objects and relay the sampled light to two infrared spectrographs. Construction is under way in collaboration with Kyoto University, the UK, and the Anglo-Australian Observatory (AAO), and is to be commissioned in 2005. MOIRCS is a fully cryogenic double beam multi-object infrared camera and spectrograph that is presently being constructed as a joint project of NAOJ and Tohoku University. First light for the camera section is expected in 2004.

A five year project to upgrade the currently offered AO system was approved and a special Grant-in-Aid for the Promotion of Science has been awarded by the Ministry of Education, Science, Culture, Sports and Technology. The new system will have five-times more control elements, increasing the Strehl ratio of the point spread function. Development of a laser guide star system is another key feature of this project, and will increase the sky coverage of the AO system.

To improve operational efficiency and optimize the observation programs according to the weather conditions, service observation will be offered on a limited scale from S03A, and flexible scheduling is under investigation. Use of the optical Cassegrain secondary mirror for the Nasmyth focus by applying active deformation of the primary mirror to remove any spherical aberration is also currently under investigation as a means to reduce the need to exchange the secondary mirrors. Like every other telescope, there are many on-going improvements on Subaru Telescope and its instrumentation, and some of the descriptions of the present paper will definitely be-

come out of date soon. The most recent information on Subaru Telescope can be checked at the following web site: http://subarutelescope.org/index.html. Readers are encouraged to obtain the most recent information from this site and/or direct contact to the Subaru Telescope staff.

76

94.5

6. Acknowledgements

440

553

The Subaru Telescope project has been a tremendous undertaking that has become a working reality through the dedication of the many people involved. Besides the astronomers, engineers, and administrative staff of NAOJ, there are many scientists from other universities, administrative staff from the Japanese government, and engineers and managing staff from contracted industries, who played valuable roles in various parts and stages of the project. All of the people who contributed to the construction and operation of the Subaru Telescope are greatly appreciated.

The project team owes much among others to Drs. D. Hall, R. MacLaren, and A. Tokunaga of the Institute of Astronomy, University of Hawaii, for their determined promotion of Subaru Telescope project, Dr. S. Okamura of University of Tokyo, Drs. H. Ohtani and T. Maihara of Kyoto University for their essential contribution to support the project.

Special thanks are extended to Messrs. N. Itoh, I. Mikami, and O. Sakakibara of Mitsubishi Electric Corporation for their originality and persistence to complete the telescope, Mr. K. Kawarai of Fijitsu Limited, Mr. J. Kawai of Fujitsu America, Mr. R. Smith of Corning Incorporated, Dr. S. Smith and Mr. M. Young of Contraves Brashear Corporation for their essential contributions to the success of the project.

References

Ando, H., Miyashita, A., Sakata, K., Shindo, S. & Barr, L., 1991, PASP, 103, 597

Ando, H., Noguchi, T., Nakagiri, M., Miyashita, A., & Yamashita, Y. 1989, Ap&SS, 160, 183

Hayano, Y., et al. 2003, Proc. SPIE, 4839, 32

Hayano, Y., Takami, H., Takato, N., Kanzawa, T., Kamata, Y., Nakashima, K., Iye, M., & Oya, S. 2000, Proc. SPIE, 4007, 149

Hayashi, S. et al. 1998, Proc. SPIE, 3352, 454

Itoh, N., Horiuchi, Y., Asari, K., & Hayashi, M. 1998, Proc. SPIE, Vol.3352, 850 Iwamuro, F., Motohara, K., Maihara, T., Hata, R., & Harashima, T. 2001, PASJ, 53, 355

Iye, M. 1989, Ap&SS, 160, 149

Iye, M. 1997, J. Korean Astron.Soc., 29, Suppl. 371

Iye, M. 2003, Proc. SPIE, 4834, 288

Iye, M., & Nishimura, T. 1995, Scientific and Engineering Frontiers for 8–10m Telescopes, ed. M.Iye & T.Nishimura (Tokyo: Universal Academy Press).

Iye, M., et al., 2000, PASJ, 52, 9

Iye, M., Noguchi, T., Torii, Y., Mikami, Y., Yamashita, Y., Tanaka, W., Tabata, M., & Itoh, N. 1990, Proc. SPIE, 1236, 929

Iye, M., Noguchi, T., Torii, Y., Mikami, Y., & Ando, H. 1991, PASP, 103, 712

Iye, M., & Yamashita, T. 2000, Proc. SPIE 4008, 18

Kaifu, N., 1998, Proc. SPIE, 3352, 14

Kaifu, N., et al., 2000, PASJ, 52, 1

Kamata, Y., Sato, T., & Kanzawa, T. 2003, Proc. SPIE 4837, 878

Kanzawa, T., Yutani, M., Kurakami.T., & Uraguchi, F. 2003, Proc. SPIE 4837, 420

Kashikawa, N., et al. 2000, Proc. SPIE 4008, 104

Kashikawa, N., et al. 2003, PASJ, 54, 819

Kataza, H., Okamoto, Y., Takubo, Onaka, T., S., Sako, S., Nakamura, K., Miyata, T., & Yamashita, T. 2000, Proc. SPIE 4008, 1144

Kawabata, K., et al. 2003, Proc. SPIE 4841, 1219

Kobayashi, N., et al. 2000, Proc. SPIE, 4008, 1056

Kodaira, K. 1989, Ap&SS, 160, 137

Kodaira, K. 1990, Proc. SPIE, 1236, 56

Kodaira, K. 1992, in ESO Conf., Progress in Telescopes and Instrumentation Technologies, ed. M.-H.Ulrich (Garching: ESO), 43

Kodaira, K. & Kogure, T. 1986, Ap&SS, 118, 5

Kogure, T. & Kodaira, K. 1991, Publ. Astron. Soc. Australia, 9, 52

Komiyama, Y., et al. 2003, Proc. SPIE, 4841, 152

Kosugi, G., Sasaki, T., Mizumoto, Y., Takata, T., Kawai, J. A., & Ishihara, Y. 1998, Proc. SPIE, 3349, 421

Kurakami, T., Yutani, M., Kanzawa, T., Ohshima, N., Uraguchi, F., Namikawa, K., Miyashita, A., & Kubota, S. 2003, Proc. SPIE, 4837, 465

Maihara, T., Iwamuro, F., Hall, D. N., Cowie, L. L., Tokunaga, A.T., & Pickles, A.J. 1993, Proc. SPIE, 1946, 581

Maihara, T., Ohta, K., Tamura, M., Ohtani, H., Akiyama, M., Noumaru, J., Kaifu, N., et al. 2000, Proc. SPIE, 4008, 1111

Mikami, I., et al. 1994, Proc. SPIE, 2199, 430

Mikami, I., Itoh, N., Miyawaki, K., Ando, H., & Noguchi, T. 1989, Ap&SS, 160, 173

Mikami, I., Sasaki, A., Itoh, N., Asari, K., Nishiguchi, K., & Iye, M. 1992, in Progress in Telescope and Instrumentation Technologies, ed. M.-H. Ulrich, (Garching: ESO), 67

Miyashita, A., Ogasawara, R., Takato, N., Kosugi, G., Takata, T., Uraguchi, F., Subaru Telescope Group, & Subaru Operation Group, 2003, Proc. SPIE, 4837, 255

Miyawaki, K., Itoh, N., Sugiyama, R., Sawa, M., Ando, H., Noguchi, T., & Okita, K. 1994, Proc. SPIE, 2199, 754

Miyazaki, S., et al. 2002, PASJ, 54, 833

Miyazaki, S., Sekiguchi, M., Imi, K., Okada, N., Nakata, F., & Komiyama, Y. 1998, Proc. SPIE, 3355, 363

Mizumoto, Y., et al. 2000, Proc. SPIE, 4009, 429

Motohara, K., et al. 2002, PASJ, 54, 315

Murakawa, K., et al. 2003, Proc. SPIE, 4841, 881

Nariai, K. & Takeshi, K. 1994, Proc. SPIE., 2199, 532 Noguchi, K., et al. 2002, PASJ, 54, 855

Noguchi, T., Iye, M., Kawakami, H., Nakagiri, M., Norimoto, Y., Oshima, N., Shibasaki, H., et al. 1989, Publ. Natl. Astron. Obs. Japan, 1, 49

Noguchi, T., Tanaka, W., Sasaki, T., Kaifu, N., Noumaru, J., Okita, K., Shimizu, T., & Itoh, N. 1998, Proc. SPIE, 3351, 361

Noumaru, J. 2002, Proc. SPIE, 4844, 8

Noumaru, J., et al. 1998, Proc. SPIE, 3349, 195

Ogasawara, R., et al. 2002, Proc. SPIE, 4844, 188

Ogasawara, R., et al. 2002, Proc. SPIE, 4844, 493

Ogasawara, R., et al. 2002, Proc. SPIE, 4845, 8 wide-area connection

Ogasawara, R., Chikada, Y., Mizumoto, Y., Kosugi, G., Sasaki, T., Noumaru, J., Takata, T., & Kawarai, K. 1998, Proc. SPIE, 3349, 255

Okamoto, Y., Kataza, H., Yamashita, T., Miyata, T., Sako, S., Takubo, S., Honda, M., & Onaka, T. 2003, Proc. SPIE, 4841 169

Saito, Y., et al. 2003, Proc. SPIE, 4841, 1180

Sako, S., et al. 2003, Proc. SPIE, 4841, 1211

Sasaki, A., Mikami, I., Shimoyama, N., Nishiguchi, K., Powell, W.R., Edwards, M.J., Ando, H., & Iye, M. 1994, Proc. SPIE, 2199, 156

Sasaki, T., et al. 1998, Proc. SPIE, 3349, 427

Takami, H., Takato, N., Hayano, Y., Iye, M., Kamata, Y., Minowa, Y., Kanzawa, T., & Gaessler, W. 2003, Proc. SPIE, 4839, 21

Takami, H., et al. 2003, PASJ, 56, 225

Takata, T., et al. 2000, Proc. SPIE, 4010, 181

Takato, N., Usuda, T., Tanaka, W., & Subaru Telescope Group, 2003, Proc. SPIE, 4837, 675

Tamura, M., et al., 2000, Proc. SPIE, 4008, 1153

Tamura, M., Fukagawa, M., Murakawa, K., Suto, H., Itoh, Y., & Doi, Y. 2003, Proc. SPIE, 4843, 190

Tanaka, W., Sasaki, T., Noguchi, T., Okita, K., Nakamura, K., Ito, F., Katsuki, Y., & Ishihara, S. 1998, Proc. SPIE, 3351, 478

Terada, H., Kobayashi, N., Tokunaga, A., Pyo, T.S., Goto, M., Weber, M., Potter, R., & Onaka, P. 2003, Proc. SPIE, 4841, 1306

Torii, Y., Hayashi, S.S., & Toda, M. 1998, Proc. SPIE, 3352, 808

Usuda, T., et al. 2000, Proc. SPIE, 4009, 141

Usuda, T., et al. 2003, Proc. SPIE, 4837, 831

Watanabe, M., 1987, Ann. Tokyo Astron. Obs., 2nd Series, 21, 241

Yagi, M., et al. 2003, Proc. SPIE, 4847, 322

Yamashita, T., & Nishimura, T. 2003, Proc. SPIE, 4841, 7

Yoshida, M., et al, 2000, Proc. SPIE, 4009, 240

Yutani, M., Hayashi, S., Kurakami, T., Kanzawa, T., Ohshima, N., & Nakagiri, M. 2003, Proc. SPIE, 4837, 887

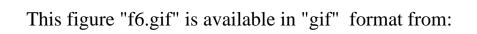
This figure "f1.gif" is available in "gif" format from:

This figure "f2.gif" is available in "gif" format from:

This figure "f3.gif" is available in "gif" format from:

This figure "f4.gif" is available in "gif" format from:

This figure "f5.gif" is available in "gif" format from:



This figure "f7.gif" is available in "gif" format from:



This figure "f9.gif" is available in "gif" format from:

This figure "f10.gif" is available in "gif" format from:

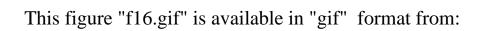
This figure "f11.gif" is available in "gif" format from:

This figure "f12.gif" is available in "gif" format from:

This figure "f13.gif" is available in "gif" format from:

This figure "f14.gif" is available in "gif" format from:

This figure "f15.gif" is available in "gif" format from:



This figure "f17.gif" is available in "gif" format from:

This figure "f18.gif" is available in "gif" format from:

This figure "f19.gif" is available in "gif" format from:

This figure "f20.gif" is available in "gif" format from:

This figure "f21.gif" is available in "gif" format from:

This figure "f22.gif" is available in "gif" format from:

This figure "f23.gif" is available in "gif" format from:

This figure "f24.gif" is available in "gif" format from:

This figure "f25.gif" is available in "gif" format from:

This figure "f26.gif" is available in "gif" format from:

This figure "f27.gif" is available in "gif" format from:

This figure "f28.gif" is available in "gif" format from:

This figure "f29.gif" is available in "gif" format from: